# Higgs-Yukawa model in chirally-invariant lattice field theory

**John Bulava**[a]**, Philipp Gerhold**[b,c]**, Karl Jansen**[c]**, Jim Kallarackal**[b,c]**,**
**Bastian Knippschild**[d]**, C.-J. David Lin**[e,f]**, Kei-Ichi Nagai**[g]**, Attila Nagy**[b,c]**, Kenji Ogawa**[h]

[a] *CERN, Physics Department, 1211 Geneva 23, Switzerland*
[b] *Institüt für Physik, Humboldt-Universität zu Berlin, D-12489 Berlin, Germany*
[c] *NIC, DESY, Platanenallee 6, Zeuthen D-15738, Germany*
[d] *Department of Physics, National Taiwan University, Roosevelt Road, Taipei 10617, Taiwan*
[e] *Institute of Physics, National Chiao-Tung University, Ta-Hsueh Road, Hsinchu 300, Taiwan*
[f] *Division of Physics, National Centre for Theoretical Sciences, Kuang-Fu Road, Hsinchu 300, Taiwan*
[g] *Kobayashi-Maskawa Institute, Nagoya University, Nagoya, Aichi 464-8602, Japan*
[h] *Department of Physics, Chung-Yuan Christian University, Chung-Li 32023, Taiwan*

## Abstract

Non-perturbative numerical lattice studies of the Higgs-Yukawa sector of the standard model with exact chiral symmetry are reviewed. In particular, we discuss bounds on the Higgs boson mass at the standard model top quark mass, and in the presence of heavy fermions. We present a comprehensive study of the phase structure of the theory at weak and very strong values of the Yukawa coupling as well as at non-zero temperature.

# I. INTRODUCTION

The Higgs-Yukawa sector of the Standard Model (SM) describes the generation of fermion masses via the non-vanishing vacuum expectation value (*vev*) acquired by the Higgs field which couples through a Yukawa coupling to the fermions. The essential element in this picture is that the coupling of the fermions to the Higgs field is chirally invariant which leads to the gauge invariant electroweak sector of the SM in the presence of gauge fields.

There are two couplings in the Higgs-Yukawa sector. They are associate with the Yukawa and the quartic scalar self-interaction operators. These couplings are directly related to the fermion and the Higgs boson masses, respectively. In the scenario that these masses are large, the corresponding couplings grow strong, and it becomes unclear whether the theory can be analysed using perturbation theory or whether non-perturbative methods must be employed. There are indeed examples where the applicability of perturbation theory is questionable. The first is the upper Higgs boson mass bound which is based on triviality arguments [1]. Here the Higgs boson mass can become large, resulting in a strong value of the quartic coupling such that perturbation theory may not work anymore. The second is the lower Higgs boson mass bound which is based on vacuum instability arguments [2–5]. Here it is unclear whether this instability is not an artefact of perturbation theory applied at large values of the Higgs field such that an expansion around the minimum of the effective potential is not justified anymore.

It is important to stress that both the lower and the upper Higgs boson mass bounds are intrinsically related to the cut-off of the theory. Thus, a calculation of the Higgs boson mass bounds can in turn be used to determine the cut-off up to which the SM is valid, once the SM Higgs boson mass has been determined. If, for example, the recent result for a scalar particle at the Large Hadron Collider (LHC) [6, 7] is confirmed as a SM Higgs boson with a mass of about 125 GeV, the SM could be valid up to very high energies before violating the Higgs boson mass bounds, see Ref. [8] for a recent analysis at next-to-next leading order of perturbation theory.

Another example where non-perturbative calculations are necessary is the possibility of a heavy fourth fermion generation [9, 10] which would lead to a large value of the corresponding Yukawa coupling. Besides these concrete examples, it is conceptually very important to study the Higgs-Yukawa sector in a non-perturbative manner since questions such as the phase structure of the model, or the spontaneous breaking of the $SU(2) \otimes SU(2)$ symmetry which underlies the Higgs mechanism are of intrinsically non-perturbative nature.

The need for a non-perturbative investigation of the Higgs-Yukawa sector of the SM has been realised already in the early 1990's. A natural choice of a non-perturbative tool is, of course, Euclidean lattice field theory. However, in these early studies, the lattice formulations of the Higgs-Yukawa sector were lacking a chirally symmetric form of the Yukawa coupling term. The absence of a chirally invariant Yukawa coupling term in the Lagrangian led to severe difficulties in studying Higgs-Yukawa model on the lattice, see Refs. [11–17] and references therein.

The situation changed however, when it was realised that –based on the Ginsparg-Wilson relation [18]– there exists a consistent formulation of an exact lattice chiral symmetry [19], which allows the chiral character of the Higgs-fermion coupling structure of the SM to be preserved on the lattice in a conceptually fully controlled manner. This triggered a number of lattice investigations of Higgs-Yukawa like models [20–28].

In this article, we report on the status of the lattice Higgs-Yukawa model using a lattice formulation that obeys an exact lattice chiral symmetry as will be explained in Sec. II. In Sec. III we will provide results for the lower and upper Higgs boson mass bounds as well as the resonance parameters of the Higgs boson [26–29]. We also extend the study of the Higgs boson mass bounds to the case of a fourth quark generation [30]. This calculation will result in rather severe constraints on the existence of a fourth fermion generation.

This article is organised as the following. In Sec. II, we describe the setting of our lattice simulations. Section III contains results of our work on the Higgs boson mass bounds in the Higgs-Yukawa model. In particular, we have investigated the effects of the fermion mass on these bounds. In Sec. IV, we present our study of the phase structure of the model. These include the bulk phase transitions at small values of the bare Yukawa coupling [23, 24], as well as in the regime of strong-Yukawa coupling [31]. We also show results and the status of our work on the finite-temperature phase structure in Sec. IV D. Finally, we conclude in Sec. V.

All statistical errors we quote in this article were obtained with a jackknife or bootstrap analysis, taking possible effects of autocorrelations fully into account. Statistical errors of the results presented in Sec. IV C have also been cross-checked using the method in Ref. [32].

## II. LATTICE SETTING AND SIMULATION STRATEGY

### A. The action

The Euclidean action of the continuum Higgs-Yukawa model containing one doublet of fermions, denoted as $t^{(c)}$ and $b^{(c)}$, and a complex scalar doublet, $\varphi^{(c)}$, is

$$S^{\text{cont}}[\bar{\psi}^{(c)}, \psi^{(c)}, \varphi^{(c)}] = \int d^4x \left\{ \frac{1}{2} \left( \partial_\mu \varphi^{(c)} \right)^\dagger \left( \partial^\mu \varphi^{(c)} \right) + \frac{1}{2} m_0^2 \varphi^{(c)\dagger} \varphi^{(c)} + \frac{\lambda_0}{4} \left( \varphi^{(c)\dagger} \varphi^{(c)} \right)^2 \right\}$$

$$+ \int d^4x \left\{ \overline{t^{(c)}} \slashed{\partial} t^{(c)} + \overline{b^{(c)}} \slashed{\partial} b^{(c)} + y_{b_0} \overline{\psi_L^{(c)}} \varphi^{(c)} b_R^{(c)} + y_{t_0} \overline{\psi_L^{(c)}} \tilde{\varphi}^{(c)} t_R^{(c)} + h.c. \right\}, \tag{1}$$

where $\tilde{\varphi}^{(c)} = i\tau_2 \varphi^{(c)}$ ($\tau_i$ are the Pauli matrices),

$$\psi_L^{(c)} = P_- \psi^{(c)} = P_- \begin{pmatrix} t^{(c)} \\ b^{(c)} \end{pmatrix} = \left( \frac{1 - \gamma_5}{2} \right) \begin{pmatrix} t^{(c)} \\ b^{(c)} \end{pmatrix},$$

$$t_R^{(c)} = P_+ t^{(c)} = \left( \frac{1 + \gamma_5}{2} \right) t^{(c)}, \text{ and similar for } b_R^{(c)}.$$

In the above equation, $m_0$ is the bare mass, $\lambda_0$ labels the bare quartic coupling, and $y_{t_0/b_0}$ denote the bare Yukawa couplings. The superscript, $(c)$, in the scalar and spinor fields indicates that these are dimensionful variables defined in the continuum. Here we stress that gauge fields are not included in our study, and we perform calculations for only one doublet of fermions throughout this work. Moreover, if not stated otherwise, the Yukawa couplings $y_{b_0}$ and $y_{b_0}$ are set equal.

It is straightforward to discretise the pure-scalar component of the above action to obtain

$$S_\Phi^{\text{latt}} = \sum_{\alpha=1}^{4} \left\{ -\sum_{x,\mu} \Phi_x^\alpha \Phi_{x+\hat{\mu}}^\alpha + \sum_x \left[ \frac{1}{2}(8 + \bar{m}_0^2) \Phi_x^\alpha \Phi_x^\alpha + \frac{\lambda_0}{4} (\Phi_x^\alpha \Phi_x^\alpha)^2 \right] \right\}, \tag{2}$$

where $x$ is a site on the space-time lattice. The symbol $\hat{\mu}$ denotes the unit vector in the space-time direction $\mu$. The mass parameter, $\bar{m}_0 = am_0$ with $a$ being the lattice spacing, is dimensionless. The real-valued field variables, $\{\Phi_x^\alpha\}$, are rendered dimensionless by a proper rescaling with $a$, and are defined on all lattice sites. These field variables are related to the discretised version of the complex scalar doublet, $\varphi^{(c)}$, in Eq. (1) through

$$a\varphi^{(\text{latt})} = \begin{pmatrix} \Phi^2 + i\Phi^1 \\ \Phi^4 - i\Phi^3 \end{pmatrix}. \tag{3}$$

It is convenient to rewrite the scalar action in Eq. (2) as

$$S_\phi^{\text{latt}} = \sum_{\alpha=1}^{4} \left\{ -2\kappa \sum_{x,\mu} \phi_x^\alpha \phi_{x+\hat{\mu}}^\alpha + \sum_x \left[ \phi_x^\alpha \phi_x^\alpha + \hat{\lambda} (\phi_x^\alpha \phi_x^\alpha - 1)^2 \right] \right\}, \tag{4}$$

with the change of variables,

$$\Phi^\alpha = \sqrt{2\kappa} \phi^\alpha, \quad \lambda_0 = \frac{\hat{\lambda}}{\kappa^2}, \quad \bar{m}_0^2 = \frac{1 - 2\hat{\lambda} - 8\kappa}{\kappa}. \tag{5}$$

For the fermions we use the action

$$S_f^{\text{latt}} = \sum_x \bar{\psi}_x \left[ D^{ov} + P_+ \phi_x^\alpha \theta_\alpha^\dagger \text{diag}(\hat{y}_t, \hat{y}_b) \hat{P}_+ + P_- \text{diag}(\hat{y}_t, \hat{y}_b) \phi_x^\alpha \theta_\alpha \hat{P}_- \right] \psi_x, \tag{6}$$

where $\hat{y}_{t/b} = \sqrt{2\kappa} y_{t_0/b_0}$, and

$$\theta_{1,2,3} = -i\tau_{1,2,3}, \ \theta_4 = 1_{2 \times 2}, \tag{7}$$

where a summation over $\alpha$ is understood. The dimensionless spinor field $\psi$ is,

$$\psi = a^{\frac{3}{2}} \begin{pmatrix} t^{(\text{latt})} \\ b^{(\text{latt})} \end{pmatrix}, \tag{8}$$

with $t^{(\text{latt})}$ and $b^{(\text{latt})}$ being the lattice version of $t^{(c)}$ and $b^{(c)}$. For the fermion kinetic term, we use the overlap operator [33–35],

$$D^{ov} = \rho \left\{ 1 + \frac{A}{\sqrt{A^\dagger A}} \right\}, \quad A = D^W - \rho, \tag{9}$$

where $\rho$ is a free, dimensionless parameter, restricted to $0 < \rho < 2r$. The locality properties of the overlap operator are optimal for $\rho = 1$ in the case of vanishing gauge couplings [35], and therefore we set it to this value in this work. The operator $D^W$ denotes the Wilson Dirac operator defined as

$$D^W = \sum_\mu \gamma_\mu \nabla_\mu^s - \frac{r}{2} \nabla_\mu^b \nabla_\mu^f, \tag{10}$$

where $\nabla_\mu^{f,b,s}$ are the (respectively) forward, backward and symmetrised lattice nearest-neighbour difference operators in direction $\mu$, and the Wilson parameter $r$ is chosen to be $r = 1$. The modified chiral projectors are given by:

$$\hat{P}_\pm = \frac{1 \pm \hat{\gamma}^5}{2}, \quad \hat{\gamma}^5 = \gamma^5 \left( 1 - \frac{1}{\rho} D^{ov} \right). \tag{11}$$

This action now obeys an exact global $\text{SU}(2)_L \times \text{U}(1)_Y$ (with $Y$ being the hyper-charge) lattice chiral symmetry with the transformations:

$$\psi \to U_Y \hat{P}_+ \psi + U_Y \Omega_L \hat{P}_- \psi, \quad \bar{\psi} \to \bar{\psi} P_+ \Omega_L^\dagger U_Y^\dagger + \bar{\psi} P_- U_Y^\dagger, \quad \phi \to U_Y \phi \Omega_L^\dagger, \quad \phi^\dagger \to \Omega_L \phi^\dagger U_Y^\dagger, \tag{12}$$

for any $\Omega_L \in \text{SU}(2)_L$ and $U_Y \in \text{U}(1)_Y$.

## B. Implementation

The actions in Eqs. (4) and (6) are used in our numerical simulations. We perform calculations on asymmetric 4-dimensional lattice volumes

$$V_4 = L_s^3 \times L_t, \tag{13}$$

where $L_s$ and $L_t$ are dimensionless spatial and temporal lattice sizes, respectively. In all our zero-temperature computations, we choose

$$L_t = 2L_s = 2L, \tag{14}$$

with $L$ typically ranging from 8 to 32. We stress that it is essential to perform computations for the Higgs-Yukawa models on large volumes. This is because the Goldstone bosons are (almost) massless and induce significant finite-size effects proportional to $L^{-2}$, in contrast to the exponential effects known for a single-particle spectrum and matrix elements for theories such as QCD with massive quarks. Figure 1 shows some examples of finite-volume effects that are present in quantities investigated in this work. It is clear from these plots that finite volume effects can be very large in the calculation of the Higgs boson mass, while they may be mild in other quantities.
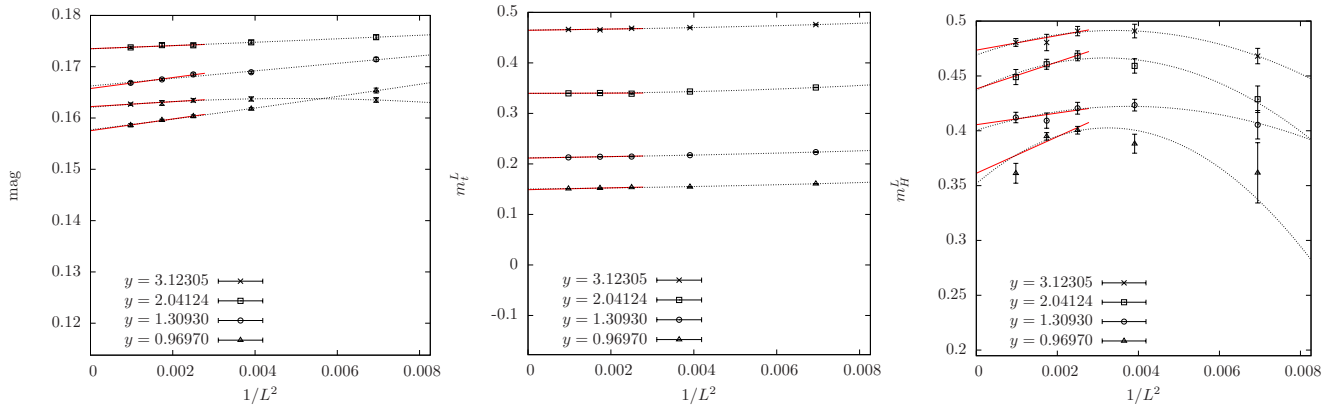
FIG. 1: Finite volume effects in the magnetisation as defined in Eqs. (15) and (16) (left), the fermion mass (middle), and the Higgs boson mass (right) at a cut-off around 1.5TeV. The data are obtained at infinite bare scalar-quartic coupling, $\hat{\lambda}$, and fermion masses in the range $m_f \approx 200 - 700$GeV. The lattice sizes used are $L = L_s = 12, 16, 20, 24, 32$. We show linear (solid lines) and quadratic (dotted lines) fits in $1/L^2$.

We implement the polynomial Hybrid Monte Carlo (pHMC) algorithm [36–38], with various improvements (see Ref. [39] for a summary), to perform non-perturbative calculations of the path integral. When compared to simulations in QCD using overlap fermions [40], it is the absence of gauge fields that makes the application of the overlap operator numerically feasible even on large lattices, as it is diagonal in momentum space.

## C. Basic observables

As described in Sec. II A, our simulations are performed using only dimensionless variables in the action. This is achieved by rescaling all the dimensionful quantities with appropriate powers of the lattice spacing, $a$. Therefore, to make connection to the real world and to have basic understanding of the spectrum of the theory, it is essential to determine the lattice spacing. This is normally carried out by computing the *vev* of the scalar field, and then setting it to the value of 246GeV. Before we describe the details of this procedure, it should be noticed that the scalar *vev* is always zero in a finite system. In principle, one would have to introduce an external source that couples to the scalar field and breaks the O(4) symmetry explicitly, and perform the infinite-volume extrapolation for every quantity computed on the lattice, before taking the source to zero. However, this procedure is numerically very demanding, and we resort to an alternative method in which we "rotate" the complex scalar doublet in every field configuration, such that its ensemble average is given by

$$\langle \hat{\phi}_{\text{rot}} \rangle = \begin{pmatrix} 0 \\ v \end{pmatrix}, \quad v = \sqrt{2\kappa} \langle m \rangle, \tag{15}$$

with

$$m = \frac{1}{V_4} \sum_x \left( \sum_\alpha |\phi_x^\alpha|^2 \right)^{1/2} \tag{16}$$

defined on each configuration. It can be shown that the magnetisation, $\langle m \rangle$, is equivalent to the scalar *vev* in the infinite-volume limit [41–43].

The renormalised scalar *vev* is given by

$$v_r = \frac{v}{\sqrt{Z_G}}, \tag{17}$$

where $Z_G$ is the Goldstone-boson wavefunction renormalisation constant. This renormalisation constant, and the Higgs-field wavefunction renormalisation constant $Z_H$, can be extracted from the momentum-space Euclidean prop-

agators of the corresponding bosons [26, 28],

$$G_{G/H}(p^2) = \frac{1}{L_t^2 \cdot L_s^6} \sum_{t_x,t_y} \sum_{\vec{x},\vec{y}} \mathrm{e}^{i\vec{p}\cdot(\vec{x}-\vec{y})+ip_4(t_x-t_y)} \left\langle \mathcal{O}_{G/H}(\vec{x},t_x) \, \mathcal{O}_{G/H}^\dagger(\vec{y},t_y) \right\rangle$$

$$\xrightarrow{p^2 \ll 1} \frac{Z_{G/H}}{p^2 + m_{G/H}^2}, \tag{18}$$

with $\mathcal{O}_{G/H}$ being the Goldstone and Higgs fields, respectively, and all the masses and momenta are in lattice units.

Through the investigation of the momentum dependence of the Goldstone boson propagator, $Z_G$ can be determined. This procedure can be improved by performing calculations in one-loop lattice perturbation theory and obtaining the propagators to this order[44]. The lattice spacing, which is related to the inverse of the cut-off scale, $\Lambda$, can now be obtained in natural units with,

$$a = \Lambda^{-1}, \quad \Lambda = \frac{246\mathrm{GeV}}{v_r}. \tag{19}$$

The masses of the bosons are given by the pole of the Euclidean propagators in Eq. (18). They can also be extracted from the time dependence of the Euclidean correlators with zero spatial momentum [26, 28],

$$C_{G/H}(\Delta t) = \frac{1}{L_t \cdot L_s^6} \sum_t \sum_{\vec{x},\vec{y}} \left\langle \mathcal{O}_{G/H}(\vec{x},t+\Delta t) \, \mathcal{O}_{G/H}^\dagger(\vec{y},t) \right\rangle$$

$$\xrightarrow{\Delta t \gg 1} A_{G/H} \exp\left(\frac{-m_{G/H}L_t}{2}\right) \cosh\left[m_{G/H} \left(\frac{L_t}{2} - \Delta t\right)\right]$$

$$\tag{20}$$

where $A_{G/H}$ are constants that are proportional to $Z_{G/H}$. This formula is valid when periodic boundary conditions are imposed. Here we stress that this method is applicable only when the ground state is the target single-particle state. Therefore, one has to be cautious when studying the Higgs boson, since it may decay into even number of Goldstone bosons. The unstable nature of the Higgs boson and the calculation of its resonance parameters will be discussed in more detail in Sec. III A.

Finally, to compute the masses of the fermions, we resort to the correlator [26, 28]

$$C_f(\Delta t) = \frac{1}{L_t \cdot L_s^6} \sum_t \sum_{\vec{x},\vec{y}} \left\langle \mathrm{Tr}\left\{ \hat{P}_- \psi(t+\Delta t, \vec{x}) \cdot \bar{\psi}(t,\vec{y}) P_- \right\} \right\rangle, \tag{21}$$

where the trace is over the spinor indices. By studying the time dependence of this correlator,

$$C_f(\Delta t \gg 1) \propto \exp\left(\frac{-m_f L_t}{2}\right) \cosh\left[m_f \left(\frac{L_t}{2} - \Delta t\right)\right], \tag{22}$$

the fermion mass can be extracted.

## III. BOUNDS ON THE HIGGS MASS

The lattice techniques described in the last section can be applied to the calculation of Higgs boson mass bounds [28, 30]. In what follows, we study the model in the broken phase, i.e. where the *vev* of the scalar field is non-zero. The Higgs boson mass is bounded from above by the triviality argument, which reflects the Gaussian nature of the fixed point of the theory. This bound is not universal and depends logarithmically on the UV cut-off of the theory. Indeed variations in the triviality bound between different lattice regularisations have been observed in the pure $\phi^4$ theory [45].

There is also an argument from perturbation theory that the Higgs boson mass is bounded from below by a vacuum-stability requirement. The picture for the lower bound in perturbation theory arises by examining the effective potential. As the fermion fields contribute negatively to the effective potential, they have a destabilising effect. By demanding the stability of the theory, this leads then to lower Higgs boson mass bounds. However, it is known that the perturbative expansion breaks down for Yukawa couplings near or less than the tree level unitarity bound [46], which is roughly 500 to 600GeV [47, 48]. In addition, the perturbative instability occurs at large values of the scalar field where an expansion around the minimum of the effective potential may not be trustworthy. Therefore it is desirable to have a non-perturbative calculation.

Although also the lower Higgs boson bound is non-universal, it is expected that it shows a much milder dependence on effects of the regularisation employed since a typical ratio $\Lambda/m_H$ is of $O(10)$ for the lower bound, while $\Lambda/m_H \sim 0.5$ for the upper bound. In the light of the recent discovery of a scalar particle at the LHC, the lower bound becomes very interesting: if this scalar particle will turn out to be the Higgs boson, the lower mass bound can be used to estimate the breakdown scale of the SM, i.e. the scale where new physics must enter to preserve the stability of the theory.

In this work, we compute the upper and lower bounds of the Higgs boson mass from non-perturbative, direct calculations using lattice field theory without relying on assumptions such as triviality or vacuum instability. From the study of the pure $\phi^4$ theory, it is known [49–52] that the Higgs boson mass is a monotonically increasing function of the quartic coupling $\lambda$ at fixed lattice spacing. This feature has been demonstrated to be present also in the Higgs-Yukawa theory [27] at fixed value of $m_f$. Therefore, in this work the lower bounds for particular values of $m_f$ and $\Lambda$ are determined at $\hat{\lambda} = 0$, while the upper bounds are obtained at $\hat{\lambda} = \infty$.

### A.   Calculating the Higgs boson mass

As pointed out in Sec. II C, calculating the mass of the Higgs boson is challenging because of its unstable nature, as it decays into even numbers of Goldstone bosons. Extracting the masses and the widths of unstable states in lattice field theory is subtle, because the theory is formulated in Euclidean space. It is further complicated by the quantisation of spatial momenta in finite volume, since the kinematics may prevent a resonance state from decaying. Therefore, a state which is unstable in infinite volume can remain a stable eigenstate in finite volume.

However, below the inelastic threshold, the infinite-volume phase shift of two-particle scattering can be determined via the investigation of finite-size effects in the energy spectrum [53]. Such finite-volume techniques for studying scattering states, albeit very challenging to implement in practice, can be used to extract resonance masses and widths in Euclidean quantum field theory [54].

In this work, we first compute the mass of the Higgs boson by assuming that its width is zero, therefore it is a stable particle in finite volume. To check this assumption, we will later use the above-mentioned finite-volume method to obtain results of the Higgs boson width, and confirm that the widths is in fact small thus not affecting the results assuming a stable Higgs boson. Under the zero width assumption, we extract the Higgs boson mass using the two approaches described in Sec. II C. Namely, we study the propagator in Eq. (18), and the correlator in Eq. (20). We then extract the Higgs boson mass by a fit of the propagator to a perturbation theory inspired formula [26, 28] and by a fit to an exponential form of the correlator of Eq. (20). The Higgs boson mass obtained in these two procedures are denoted $m_H^p$ and $m_H^c$, respectively. An example of the two methods for determining $m_H$ is illustrated in Fig. 2. We extract the fitted values $m_H^p$ and $m_H^c$ which agree within one standard deviation and both fits provide a suitable description of the data. The plots in this figure are for $m_f = 195$GeV. We note that we observe similar agreement between $m_H^p$ and $m_H^c$ for all our choices of simulation parameters.

To check the validity of the assumption that the Higgs boson is stable in our work, a calculation of the Higgs boson resonance parameters has been performed in Ref. [29]. Since the finite volume techniques proposed in Refs [53, 54] are only applicable below the inelastic threshold, external sources were introduced which give a mass to the Goldstone bosons and break the O(4) symmetry explicitly. In the calculation the Goldstone boson energies were computed at non-zero momenta, using the original center of mass frame [53, 54] as well as a moving frame [55, 56]. By adjusting the values of the external source and the momenta, the Goldstone boson energies were tuned such that

$$2E_G < m_H < 4E_G \, . \tag{23}$$

The scattering phase shifts from which the resonance parameters were extracted are shown in Fig. 3, along with the position of the inelastic thresholds. These phase shifts are used to fit the Breit-Wigner formula to determine the resonance mass and width.
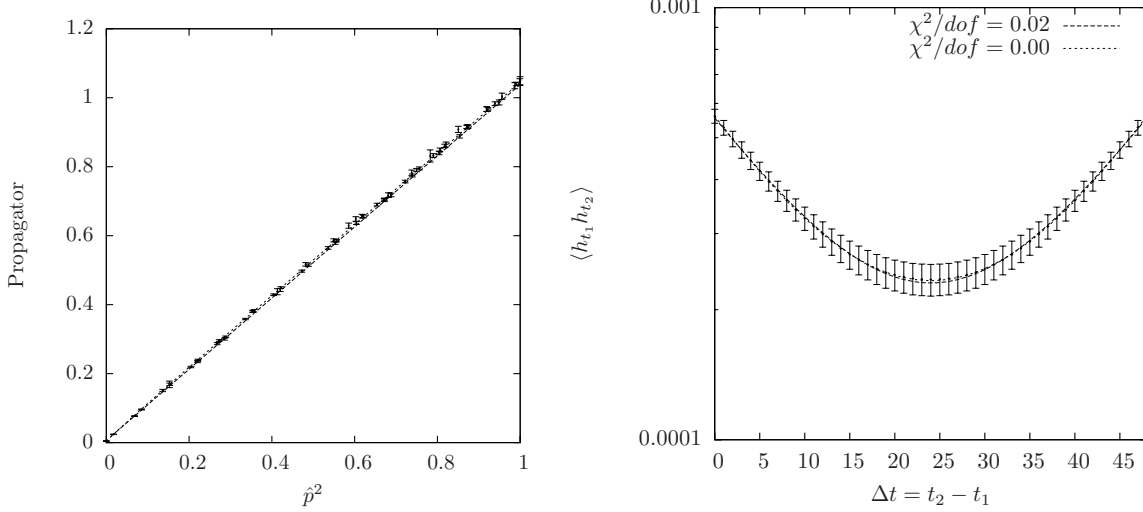


FIG. 2: Examples of fits to the Higgs momentum space propagator and the Higgs temporal correlation function to obtain $m_H^p$ and $m_H^c$, respectively. The results are from a $24^3 \times 48$ lattice with $m_f = 195\text{GeV}$, $\Lambda = 1.5\text{TeV}$. The fitted values are $m_H^p = 96.0(4.3)\text{GeV}$ and $m_H^c = 96.4(6.9)\text{GeV}$ where the errors are statistical only and do not reflect the uncertainty in the scale determination which, however, affects both values in the same way.
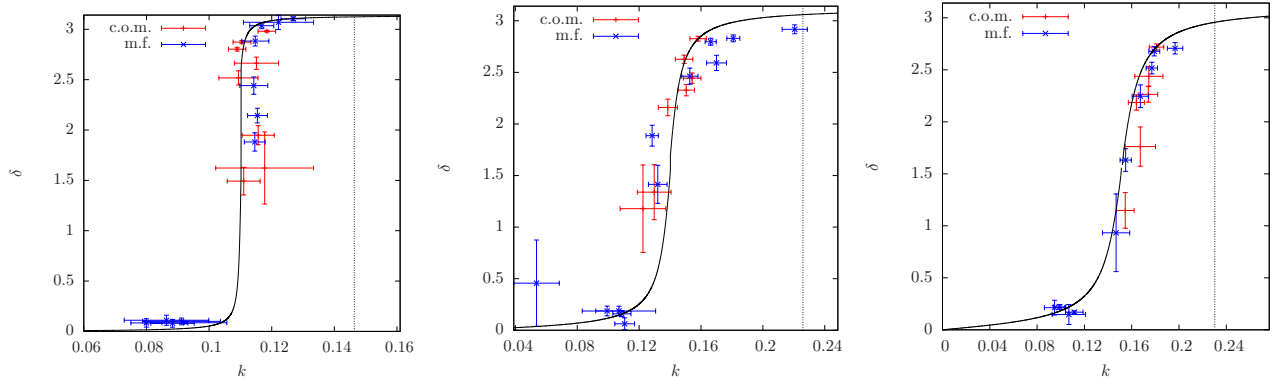


FIG. 3: Results for the scattering phase shifts at three values of $\hat{\lambda}$. From left to right, the plots correspond to $\hat{\lambda} = 0.001, 10, \infty$, respectively. In each plot, the vertical dotted line indicates the position of the four-Goldstone threshold, above which our analysis method is inapplicable. Also, points obtained from both the centre of mass system (c.o.m.) and a system with one unit of total momentum (m.f.) are shown. Taken from Ref. [29].

The results of the Higgs boson width and mass obtained via the resonance analysis, perturbation theory, using the time-slice correlator and employing the momentum space Higgs boson propagator are shown in Tab. I. Here, the top quark mass has been set to its physical value. It is clear that the Higgs boson mass determined by the resonance study is consistent with that extracted from fits to the momentum space propagator and the temporal correlation function. Furthermore, we see that at $m_f = m_t$, the width of the Higgs resonance is narrow, i.e. at most $\sim 10\%$ of the resonance mass in all cases. From the results presented in this table, it is demonstrated that it is justifiable to assume that the Higgs boson width is zero since it turns out to be very narrow in the resonance analysis such that the width has no effect on the mass extraction.

| $\hat{\lambda}$ | $\Lambda$ [GEV] | $m_H^{\text{resonance}}$ | $\Gamma_H^{\text{resonance}}$ | $\Gamma_H^{\text{pert}}$ | $m_H^p$ | $m_H^c$ |
|---|---|---|---|---|---|---|
| 0.01 | 883(1) | 0.278(3) | 0.0018(14) | 0.0054(1) | 0.278(2) | 0.274(4) |
| 1.0 | 1503(5) | 0.383(6) | 0.0169(4) | 0.036(8) | 0.386(28) | 0.372(4) |
| $\infty$ | 1598(2) | 0.403(6) | 0.037(9) | 0.052(2) | 0.405(4) | 0.403(7) |

TABLE I: The results (taken from Ref. [29]) of a study comparing the resonance parameters of the Higgs boson with the results of fits to the temporal correlation function and momentum space Higgs boson propagator. Errors are statistical only. Except for the cut-off scale, all the results are in lattice units. The fermion mass is set to be the physical top-quark mass. Results from three values of the quartic coupling are presented. Also shown are the resonance mass and width from Breit-Wigner fits to the scattering cross-section. Finally, a perturbative estimate of the resonance width is included. We note that because of some data losses the error on $m_H^p$ at $\hat{\lambda} = 1.0$ is larger than for the other parameters.

## B.    Results of the Higgs boson mass bounds

We now turn to the results of the Higgs boson mass bound calculations discussed in the previous section. We first discuss the results of Ref. [28], where the upper and lower bounds were computed at several choices of the cut-off scale, with the fermion masses at the physical top-quark mass, and also at $m_f \sim 676$GeV. The main result from Ref. [28] is shown in Fig. 4. In the left graph, the situation for a SM top quark mass is shown. The right graph shows the situation for a fermion mass of $m_f \sim 676$GeV. It can be clearly seen that while the upper bound is relatively unaffected when using a heavy fermion mass, the lower bound increases substantially.
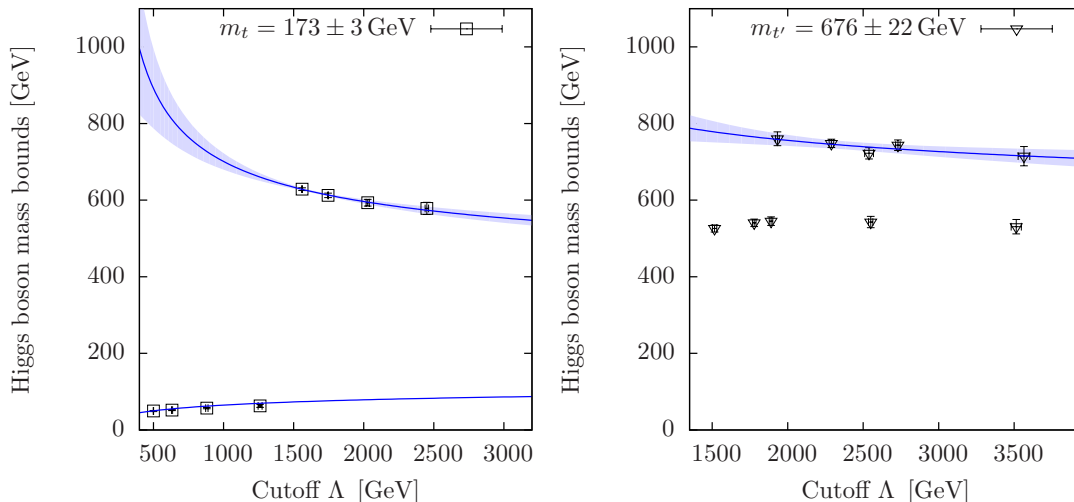


FIG. 4: The cut-off dependence of the upper and lower Higgs boson mass bounds for fermion mass at $\sim$ 173GeV (left) and $\sim$ 676GeV (right). All data have been extrapolated to infinite volume.

Apart from the cut-off dependence of the bounds at a fixed value of $m_f$, the dependence of the bounds on $m_f$ itself has also been examined at a fixed value of the lattice cut-off [57], the results of which are shown in Fig. 5 (left). We clearly observe the increase of the lower bound with increasing $m_f$ in this figure. In particular, Fig. 5 suggests that with a Higgs boson mass of $\sim$ 125GeV, the mass of a mass-degenerate fourth generation of quarks is restricted to be less than $\sim$ 350GeV. This is clearly already below the bounds from direct experimental searches.
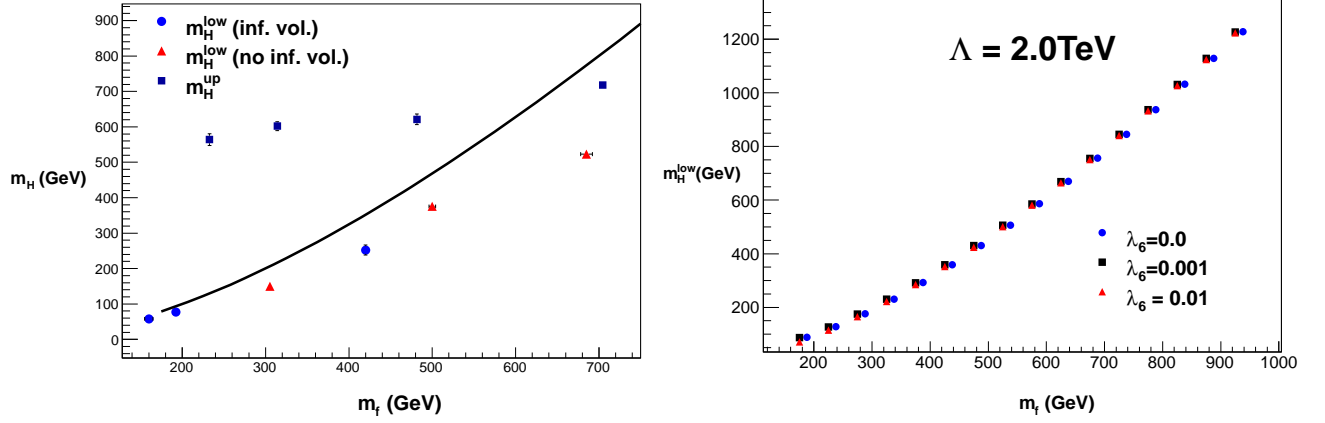
FIG. 5: Left: The dependence on the fermion mass of the upper and lower Higgs boson mass bounds, at the cut-off scale $\Lambda = 1.5$TeV. Data points from lattice calculations are shown. Results for the lower bound without infinite-volume extrapolation, using only $24^3 \times 48$ lattices, are also shown for comparison. The solid line results from a one-loop calculation of the effective potential, as explained in the text. Right: effects of a $\phi^6$ operator with coupling $\lambda_6$ for the lower bound of the Higgs boson mass, at various fermion masses and the cut-off scale $\Lambda = 2$TeV. Three values of the coupling constant $\lambda_6$ are plotted.

In addition to the numerical results, Fig. 5 also contains the estimate of the lower bound from an effective potential calculation, which was performed using the same lattice regularisation as in our Monte Carlo simulation. In this calculation, the effective potential was computed to one-loop order in the large$-N_f$ limit. Operationally, the one-loop calculations were carried out by numerically computing the required momentum-mode summations in a series of finite lattice volumes, and then extrapolating to the infinite-volume limit. From this one-loop effective potential, $V$, the Higgs boson mass is determined by solving for the scalar $vev$, $v$, and the Higgs boson mass in the gap equations,

$$\frac{d}{d\phi}V(\phi)|_{\phi=v} = 0, \quad \frac{d^2}{d\phi^2}V(\phi)|_{\phi=v} = m_H^2 . \tag{24}$$

To compare to the numerically computed lower Higgs boson mass bound, in the effective potential calculation the quartic coupling has been set to zero. In addition, the cut-off and the fermion mass were fixed to the same values as in the simulations such that a direct comparison is possible. For a standard model top quark mass it has been demonstrated in [26, 27] that the lattice effective potential provides an excellent description for the numerical data for the lower Higgs boson mass bound.

The left panel of Fig. 5 clearly demonstrates that the trend of an increasingly higher value of the lower bound with increasing fermion masses, as suggested by the perturbative calculation is realised by the data up to very large values of $m_f$, although the quantitative agreement is better at low $m_f$. Based on this qualitative agreement, we can examine the effect of higher-dimensional operators in the effective potential using the same loop and $1/N_f$ expansion. To this end we include the contribution from the operator $\lambda_6\phi^6$ in the effective potential with $\lambda_6$ the coupling constant. The addition of such an operator in the Lagrangian modifies the solution to Eq. (24), and can therefore alter the lower bounds on the Higgs boson mass in principle.

Here we stress that the cut-off cannot be removed in the Higgs-Yukawa model. Furthermore, any perturbative expansion in this model is only valid in the regime where the cut-off scale, $\Lambda = 1/a$, is large enough compared to low-energy scales such as the Higgs boson mass and the scalar $vev$. In Ref. [49], it was demonstrated that $m/\Lambda < 0.5$ (with $m$ being a typical low-energy scale) is enough to ensure the applicability of perturbation theory to the pure $\phi^4$ scalar field theory. Here we impose the same condition, but on the value of the scalar field, in our perturbative calculation for the effective potential for the Higgs-Yukawa model including the $\lambda_6\phi^6$ operator. This results in the stability criterion

$$\frac{d^2}{d\phi^2}V(\phi) > 0, \quad \phi < 0.5, \tag{25}$$

where $\phi$ has been properly rescaled to be in lattice units.

In the right panel of Fig. 5, we show the results of our investigation of the lower bounds on the Higgs boson mass, using the one-loop effective potential including the contribution from the $\lambda_6 \phi^6$ operator. It is clear that in the regime where the perturbative expansion is valid, a wide range of values of $\lambda_6$ lead to qualitatively very similar results. Finally, we also point out that exploratory numerical Monte Carlo simulations which include the $\phi^6$ operator agree with the perturbative results for a large range of bare Yukawa couplings [27].

## IV. STUDY OF THE PHASE STRUCTURE

### A. Purposes and strategy of the study

It is an important task to explore the phase structure of the Higgs-Yukawa model to identify the phase structure of the theory and determine the critical coupling constant values where a continuum limit can be performed. In this section, we will discuss two aspects concerning the phase structure of the Higgs-Yukawa model considered here. The first are the locations of second-order bulk phase transitions in the bare parameter space which can be identified as the continuum limits of the lattice theory. For weak values of the bare Yukawa coupling the phase structure has been investigated in [23, 24] and its knowledge was very helpful to identify the simulation parameters for the desired physical situation, i.e. a fixed value of the cut-off and the physical values of the fermion masses. Here we remark that the bounds on the Higgs boson and fermion masses as presented in Fig. 5 in Sec. III B are obtained in this weak bare Yukawa coupling regime. In this section, we focus now on the large bare Yukawa coupling region and explore the phase structure of the theory in this regime of the parameter space. The aim is to investigate, whether the phase transitions at large bare Yukawa coupling are governed by the same, Gaussian fixed point as at small Yukawa coupling. If we would find deviations from the Gaussian fixed point behaviour, this would open the possibility that the renormalised Yukawa coupling can remain strong up to a high cut-off scale which could lead to heavy fermion masses and even the existence of bound states. We have therefore been performing simulations at large values of bare Yukawa coupling[1], and the exploratory results will be presented in Sec. IV C. As a second aspect, we will present an investigation of the finite-temperature phase transition in understanding the role of, in particular, heavy fermion masses for the electroweak phase transition, especially with respect to questions concerning baryogenesis [60].

Before detailing our on-going studies of the bulk and thermal phase transitions of the Higgs-Yukawa model in the following two sections, here we describe the general strategy in this work.

It is natural to use the *vev* of the scalar field to probe the phase structure. However, a naive computation of this *vev* will always lead to vanishing results in lattice calculations even in the broken phase, because of the finite volume as used in the simulations. As discussed in the beginning of Sec. II C, it is appropriate to replace the scalar *vev* with the magnetisation as defined in Eqs. (15) and (16).

In order to probe the nature of phase transitions, we have to determine anomalous dimensions of the operators allowed by the symmetries. In finite volume, second-order phase transitions are washed out and become cross-overs, and the correlation length cannot exceed the size of the system. Therefore, for the study of the phase structure, we resort to finite-size scaling techniques. These techniques were developed originally by solving the renormalisation group equation (RGE) for finite-volume lattice systems in condensed matter physics [61]. To draw analogy between field theory and statistical mechanics, we also refer to these anomalous dimensions by calling them critical exponents in this article, as usually done in statistical mechanics.

It is challenging to determine the anomalous dimension of the operator corresponding to the Yukawa coupling term, because of the presence of fermions and the flavour-changing structure of the operator. We will postpone the discussion of this operator for future reports. Here we focus on critical exponents in the scalar sector. To start, we calculate the susceptibility,

$$\chi_m = V_4 \left( \langle m^2 \rangle - \langle m \rangle^2 \right), \tag{26}$$

---

[1] In Ref. [58, 59], it was demonstrated that in the limit where the bare Yukawa coupling becomes infinity, the Higgs-Yukawa model is equivalent to the pure O(4) scalar model. However, our simulations are performed away from this limit.

which is the connected two-point function in the scalar sector. This quantity is proportional to the square of the correlation length, $\xi$, and diverges at second-order phase transitions in the infinite-volume limit. Solving the RGE for this correlator for a finite-size system at fixed cut-off scale (lattice spacing) near a second-order phase transition, one obtains the scaling law,

$$\chi_m\left(t, L_s\right) \cdot L_s^{-\gamma/\nu} = g\left(t L_s^{1/\nu}\right), \text{ with } t = (T/T_c - 1) \tag{27}$$

where $g$ is a universal scaling function, $L_s$ is the spatial extent of the lattice, and $T_c$ is the critical temperature in the infinite-volume limit, which could also be represented by the critical value of a particular coupling. The critical exponents, $\gamma$ and $\nu$ are related to the anomalous dimensions of the scalar field and the mass operator, $\phi^2$. This scaling behaviour is exact near the critical point for space-time dimension, $d < 3$. Therefore it is an appropriate tool in our study of the finite-temperature phase transition. However, in the investigation of the bulk phase structure, we have a $d = 4$ field theory, and the above scaling relation should be modified because of triviality [62–66], if the transition is governed by a Gaussian fixed point. These modifications appear as logarithmic corrections in Eq. (27). They are not included in the analysis presented in this article, but are being considered in our on-going work.

As will be discussed in the following, the scaling tests and the extraction of anomalous dimensions using Eq. (27) are complicated because of the number of free parameters that are involved in the methods for modelling the unknown universal function, $g$. In particular, it is difficult to accurately determine $\nu$ using this procedure. This complication can be reduced by studying Binder's cumulant [67],

$$Q_L = 1 - \frac{\langle m^4 \rangle}{3 \langle m^2 \rangle^2}. \tag{28}$$

This quantity is simply the connected four-point function, normalised by the square of the two-point function, in the scalar sector. Because of the normalisation, $Q_L$ is independent of the critical exponent $\gamma$. Furthermore, it is related to the renormalised scalar quartic coupling in the infinite-volume limit by a proportionality factor $V_4/\xi^4$ [68]. Since Binder's cumulant is normalised to be dimensionless, its values computed on different (dimensionless) lattice sizes with the same cut-off scale will coincide with each other at the critical point. It is also expected to exhibit milder scaling violations resulting from higher-dimensional operators [69, 70].

In the next three sections, we discuss details of the investigation of the thermal and bulk phase structures using the quantities defined in this section. Errors on all the numerical results in this section are statistical only.

## B. Bulk phase structure at small Yukawa couplings

Before reporting the details of our on-going investigation in the bulk phase structure of the Higgs-Yukawa model in the strong-Yukawa regime, we briefly summarise the results obtained in the region of weak-Yukawa coupling [24] in this section. The order parameters characterising the different phases are the magnetisation defined in Eqs. (15) and (16), and the staggered magnetisation

$$\langle s \rangle = \left\langle \frac{1}{V_4} \sum_x (-1)^{x_1 + x_2 + x_3 + x_4} \left( \sum_\alpha |\phi_x^\alpha|^2 \right)^{1/2} \right\rangle. \tag{29}$$

The staggered magnetisation is relevant for the breaking of the symmetry,

$$\begin{aligned} \kappa &\longrightarrow -\kappa, \\ \phi_x^\alpha &\longrightarrow (-1)^{x_1 + x_2 + x_3 + x_4} \phi_x^\alpha, \end{aligned} \tag{30}$$

in the action in Eq. (4).

In the Higgs-Yukawa model, four phases have been observed:

1. A symmetric (SYM) phase with $\langle m \rangle = \langle s \rangle = 0$.

2. A broken, or ferromagnetic (FM), phase with $\langle m \rangle \neq 0$ but $\langle s \rangle = 0$.

3. A staggered-broken, or anti-ferromagnetic (AFM), phase with $\langle m \rangle = 0$ but $\langle s \rangle \neq 0$.

4. A ferrimagnetic (PI) phase with $\langle m \rangle \neq 0$ and $\langle s \rangle \neq 0$.

Our current knowledge of the phase structure of the Higgs-Yukawa model in the weak-Yukawa regime is summarised in Fig. 6. To make it convenient in comparing results from numerical simulations to a large$-N_f$ analytic calculation [23], we have performed the change of variables,

$$\hat{y} = \frac{\tilde{y}_N}{\sqrt{N_f}}, \quad \kappa = \tilde{\kappa}_N, \quad \hat{\lambda} = \frac{\tilde{\lambda}_N}{N_f}, \quad \Phi = \sqrt{N_f}\tilde{\Phi}, \tag{31}$$

in the plots in this figure. The large$-N_f$ calculation was carried out in the $N_f \to \infty$ limit while keeping $\tilde{y}_N$, $\tilde{\lambda}_N$ and $\tilde{\Phi}$ fixed. The left panel of Fig. 6 is the result from the large$-N_f$ calculation, and the middle panel is the comparison between this calculation and the numerical results from lattice simulations at $N_f = 10$. The right panel of this figure shows the $N_f$ dependence on the critical values of $\kappa$ at the SYM$-$FM and FM$-$AFM transitions in our numerical calculation, with the Yukawa coupling set to $\tilde{y}_N = 0.1$. It is observed that the $N_f$ dependence appears to be mild. This indicates that the large$-N_f$ analytic calculation may serve as a reasonable, qualitative, guide in choosing the simulation parameters for the numerical simulations. Although this analysis has been performed in the weak Yukawa coupling region, the good qualitative description makes it possible to also use the large $N_f$ expansion also in the strong-Yukawa regime, which was indeed observed in [23].
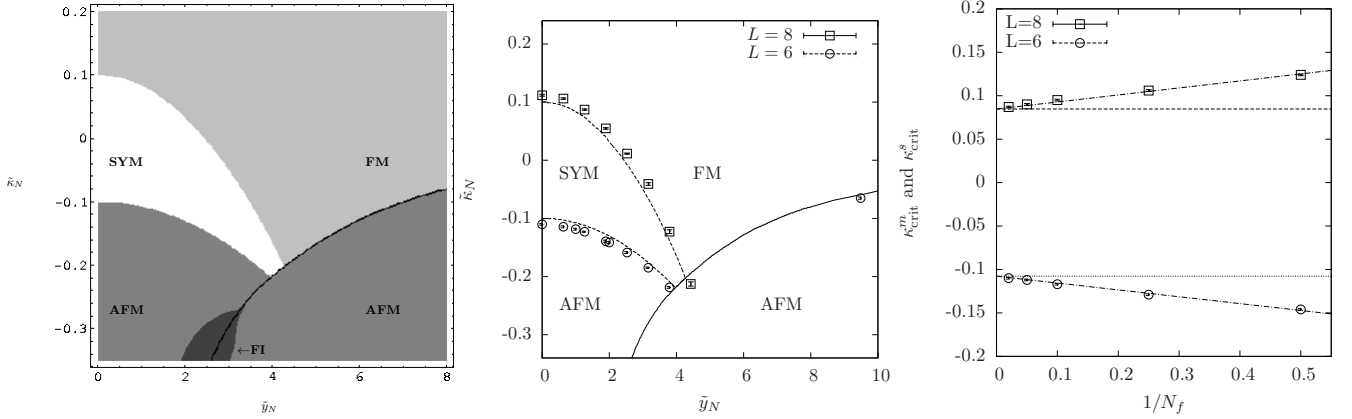


FIG. 6: The phase structure analysis. The left panel shows analytical predictions for the case of $L_s = \infty$, $N_f = \infty$ and $\tilde{\lambda}_N = 0.1$. The black line indicates a first order phase transition, while all other transitions are of second order. The middle panel demonstrates a numerical test of the transitions from the SYM to both FM and AFM phases with $N_f = 10$. The right panel displays the $N_f$ dependence in the critical values of $\kappa$ for the SYM$-$FM and SYM$-$AFM transitions, at $\tilde{\lambda}_N = 0.1$ and $\tilde{y}_N = 1.0$. These critical $\kappa$ values are denoted as $\kappa_{\rm crit}^m$ ($> 0$) and $\kappa_{\rm crit}^s$ ($< 0$), respectively. The squares and circles in the middle and right panels of the figures come from direct numerical simulations on the indicated lattice sizes.

In the weak Yukawa coupling region, we concentrated on the study of the SYM$-$FM phase transition, which was confirmed to be second-order. This allowed us to study physically interesting quantities, such as the Higgs boson mass bound presented in Sec. III, near this phase-transition with good control of the cut-off dependence.

## C. Bulk phase transition at large Yukawa couplings

It is not well understood how the Higgs-Yukawa model at large bare Yukawa couplings differs from that in the weak-coupling regime. A first step in a detailed analysis and hence a deeper understanding of the model in this region is the investigation of the bulk phase transitions. It can be shown that the Higgs-Yukawa model reduces to a pure

scalar non-linear $\sigma$-model at infinite bare Yukawa couplings [58, 59], and hence becomes trivial at a certain cut-off scale. However, it is not clear what happens at large but finite Yukawa couplings. To be able to detect any differences from a Gaussian (trivial) theory the critical exponents of the phase transition have to be extracted and compared with those of the O(4) model. If the strong-coupling regime is indeed different from the weak-coupling one and hence would be governed by a non-trivial fixed point[2], it would be very interesting to investigate the possibility of very heavy fermions which give rise to a fourth generation, while still maintaining a light Higgs boson in the theory. In such a scenario it is unclear, whether an analysis as, e.g. [72] is applicable and also, whether the Higgs boson mass bounds of section III are valid.

The magnetisation, defined in Eqs. (15) and (16), can act as an order parameter to identify and determine the order of the phase transition. In Fig. 7, the magnetisation for the Higgs-Yukawa model obtained on different lattice volumes is shown as a function of $y$ for two $\kappa$ values. In addition, we show the magnetisation as a function of $\kappa$ for the O(4) model. The SYM and FM phases can be clearly distinguished and the phase transition is washed out because of finite volume effects as previously discussed.

The absence of any discontinuities in the magnetisation is strong evidence for a second-order phase transition in all three depicted cases. In general, second-order phase transitions are classified through their critical exponents and the question arises if these exponents are different in the strong-Yukawa and pure O(4) models. To answer this question, a careful investigation of the susceptibility and Binder's cumulant will be presented in the following.



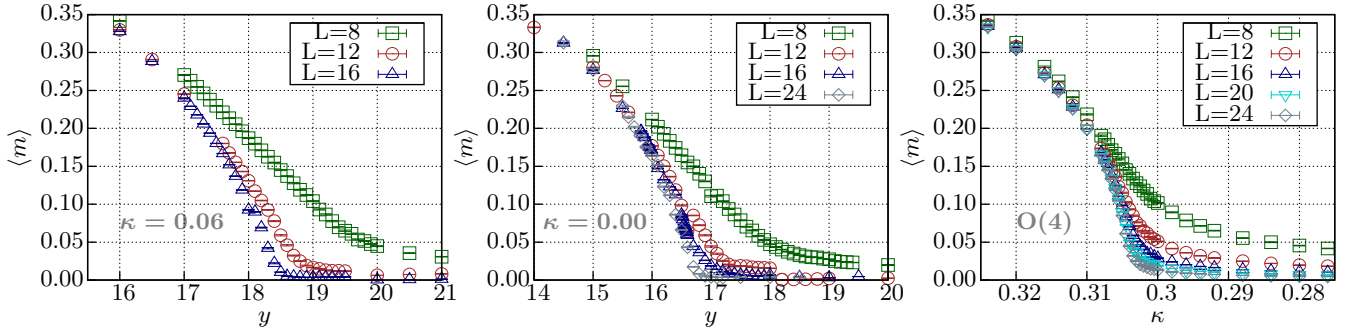FIG. 7: Magnetisation, $\langle m \rangle$, for the Higgs-Yukawa model at $\kappa = 0.06$ (left), $\kappa = 0.00$ (middle) and the pure O(4) model (right) for various volumes. For the O(4) $\langle m \rangle$ is plotted as a function of *decreasing* $\kappa$ to match optically with the Higgs-Yukawa model. The absence of discontinuities in $\langle m \rangle$ is an evidence for a second order phase transition.

The critical exponents can be calculated by using the finite-size scaling of the susceptibility, Eq. (26). The susceptibility is shown in Fig. 8 for the Higgs-Yukawa and O(4) models. This quantity diverges at the critical point in the infinite volume limit. Such a divergence in infinite volume is reflected in a bulk finite-size scaling behaviour in lattice calculations. As mentioned before in Eq. (27), the finite-size scaling is predicted by renormalisation group theory, with modifications resulting from scaling violation such as that discussed in Ref. [61],

$$\chi_m\left(t, L\right) \cdot L_s^{-\gamma/\nu} = g\left(\hat{t} L_s^{1/\nu}\right), \text{ with } \hat{t} = \left[T/\left(T_c^{(L=\infty)} - C \cdot L_s^{-b}\right) - 1\right], \tag{32}$$

where $C$ is a phenomenological parameter and $b$ is a shift exponent [61]. This modification comes from the fact that the position of the maximum of $\chi_m$ is volume dependent. From Eq. (27) the infinite-volume critical temperature can be extracted directly. For the O(4) model we do not observe any shift of the maximum and hence Eq. (27) is a good description of our data in this case. It should be stressed, that the temperature, $T$, in this section is the control parameter. In our work, it is either the Yukawa coupling, $y$, in the Higgs-Yukawa model or the hopping parameter,

---

[2] There has been early lattice work on the 3-dimensional Higgs-Yukawa model [71], attempting at finding fix points that are different from that of the pure scalar field theory.

$\kappa$, in the pure O(4) model. To extract the critical exponents from the susceptibility, we perform a simultaneous fit of all data obtained at all volumes to the partly-empirical formula [73],

$$\chi_m = A \left( L_s^{-2/\nu} + B \left[ T/T_c^{(L=\infty)} - C \cdot L_s^{-b} - 1 \right]^2 \right)^{-\gamma/2}. \qquad (33)$$

This formula was also used for a fit to $\chi_m$ of the O(4) model, but with the modification of excluding the parameters $C$ and $b$ because of the reasons mentioned above. The fit results are summarised in Tab. II and will be discussed later. Notice that there may be logarithmic corrections to the scaling behaviour of the susceptibility because triviality may still be present also in the strong-Yukawa model. These corrections should, in principle, be included in Eq. (33)[3]. This is on-going work, and the result will be presented in a later publication. Therefore, we consider our present values of the critical exponents as preliminary and they should be taken with caution.
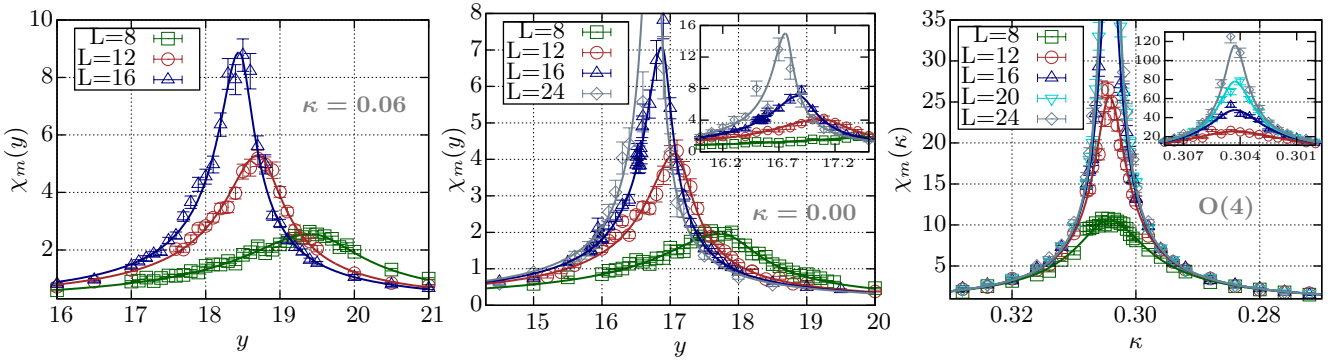


FIG. 8: Susceptibility $\chi_m$ at $\kappa = 0.06$ (left), $\kappa = 0.00$ (middle) and the O(4) model (right) for various volumes. The curves are the result of a fit to Eq. (33). The right top boxes in the middle and the right panels show $\chi_m$ for the largest volumes. For the Higgs-Yukawa model a volume-dependent shift of $y_c$ towards $y_c^{(L=\infty)}$ can be observed. This shift is not observed in the O(4) model.

| | $T_c^{(L=\infty)}$ | $\nu$ | $\gamma$ | $C$ | $b$ | fit interval |
|---|---|---|---|---|---|---|
| $\kappa = 0.06$ | 18.119(67) | 0.576(28) | 1.038(30) | 4.7(1.6) | 1.95(18) | 17.5, 20.0 |
| $\kappa = 0.00$ | 16.676(15) | 0.541(22) | 0.996(15) | 10(2) | 2.42(10) | 15.0, 19.0 |
| O(4) | 0.304268(27) | 0.499(12) | 1.086(19) | N/A | N/A | 0.300, 0.308 |

TABLE II: Results of a correlated fit to the susceptibility according to Eq. (33) where the last column indicates the fit interval. The parameter $T$ stands either for $y$ in the Higgs-Yukawa model or for $\kappa$ in the O(4) model. Since no volume-dependent shift can be observed in the O(4) model for $\chi_m$, the parameters $C$ and $b$ have not been fitted here. All quoted errors are statistical only.

It is possible to re-scale the susceptibility according to Eq. (32) for the Higgs-Yukawa theory, or Eq. (27) for the O(4) model, respectively. The fitted parameters extracted from Eq. (33) can be used to construct $\chi_m(t, L_s) \cdot L_s^{-\gamma/\nu}$ and test its scaling against $t \cdot L_s^{1/\nu}$. This is shown in Fig. 9. Points for all volumes collapse on the same curve in each of the three cases shown. This behaviour is typical for second-order phase transitions and hence provides further evidence that such a second-order transition happens in the regime of strong Yukawa couplings.

---

[3] These logarithmic corrections are surely present in the finite-size scaling behaviour of the susceptibility in the pure O(4) model [62–66]. However, our exploratory numerical results show that their inclusion produces minor changes in the results of the critical exponents in the O(4) model.

An alternative way of determining critical exponents is via Binder's cumulant, Eq. (28). One advantage of this quantity over the susceptibility is its milder power-law scaling violation which is given by

$$Q_L = g_{Q_L}\left(t L^{1/\nu}\right), \tag{34}$$

where $g_{Q_L}$ is a universal function and $t$ is defined in Eq. (27). This behaviour can be observed in Fig. 10 where all volumes intersect at the phase transition point in infinite volume where $t = 0$. Even for the Higgs-Yukawa model no shift can be observed and hence the parameters $C$ and $b$ can be completely neglected in the scaling variable.
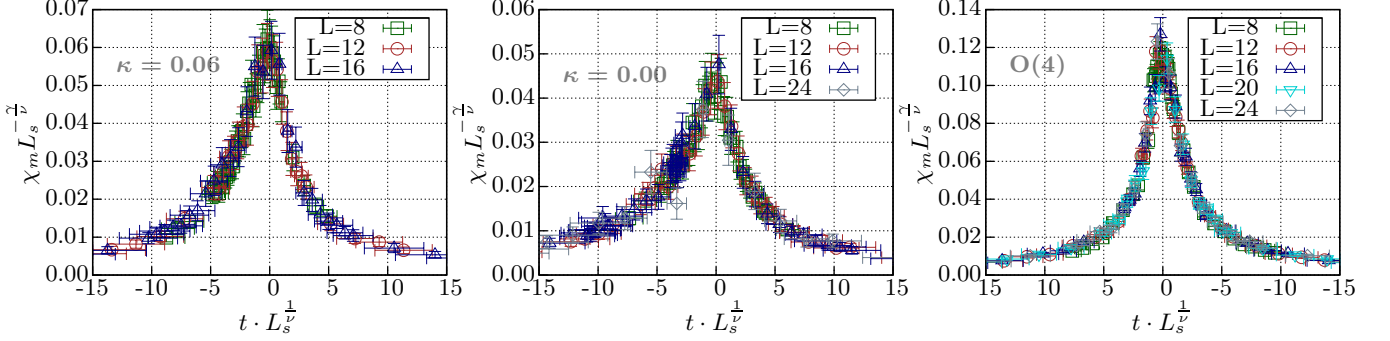


FIG. 9: Scaling behaviour of susceptibility at $\kappa = 0.06$ (left), $\kappa = 0.00$ (middle) and the O(4) model (right) for various volumes.

The value of Binder's cumulant in the broken phase comes from the fact that $\langle m^4 \rangle \approx \langle m^2 \rangle^2$ and hence $Q_L \approx 2/3$ [67]. Our results for $Q_L$ at the critical point come close to this value for all setups considered here. Still, $Q_L$ obtained in the Higgs-Yukawa model differs from the one in the O(4) model. This may arise from effects of finite renormalisation because of the inclusion of fermions. Its implication in the difference of the O(4) model and the Higgs-Yukawa model is under investigation now. Furthermore, it can be demonstrated that for Binder's cumulant, as contrary to the susceptibility, there is no logarithmic corrections to the scaling behaviour arising from triviality in the pure O(4) model [64]. Whether or not such corrections can be present in the Higgs-Yukawa model is being studied now.
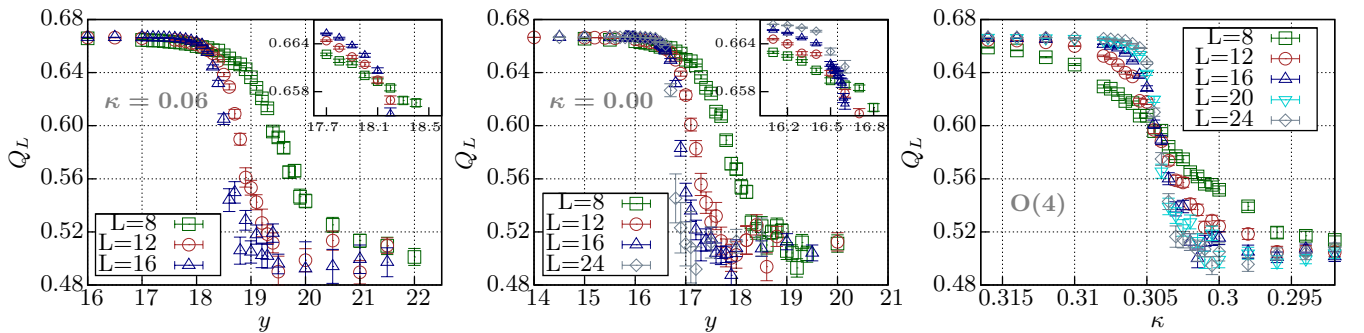


FIG. 10: Binder's Cumulant $Q_L$ at $\kappa = 0.06$ (left), $\kappa = 0.00$ (middle) and the O(4) model (right) for various volumes where the subscript L indicates the finite volume quantity. Note that the value of $Q_L$ at the critical point is different in the Higgs-Yukawa and the O(4) models.

The basic idea of extracting the critical exponent, $\nu$, from Binder's cumulant is the use of the curve collapse of Eq. (32). If the scaling function $g_{Q_L}$ is known one will simply minimise [74]

$$R_{Q_L} = \frac{1}{N} \sum \left| Q_L - g_{Q_L}\left(t L^{1/\nu}\right) \right|, \quad (N = \text{total number of data points}) \tag{35}$$

which would allow to extract $\nu$ as a direct consequence of the scaling behaviour. The sum is taken over all data points, and $R_{Q_L}$ is minimal for the correct choice of the parameters $\nu$ and $T_c^{L=\infty}$. In the absence of any statistical and systematic errors the function $R_{Q_L}$ would become zero.

The scaling function $g_{Q_L}$ is unknown. However, this can be overcome by the observation that any volume, in the following called $p$, can act as a reference function for the correct choice of parameters, taking thus over the role of $g_{Q_L}$. Instead of minimising Eq. (35), we minimise [74]

$$P_b = \left[ \frac{1}{N_{\text{over}}} \sum_p \sum_{j \neq p} \sum_{i,\text{over}} \left| Q_{L_j} - \mathcal{E}_p \left( t_{ij} L_j^{1/\nu} \right) \right|^2 \right]^{1/2} . \tag{36}$$

Here, the scaling function is replaced by the interpolating function $\mathcal{E}_p$ which is constructed by interpolating the data points obtained on volume $p$ to volume $j$ for the values of the scaling variable $t_{ij} L_j^{1/\nu}$, with the index $i$ going through all data points of volume $j$. In our case, $\mathcal{E}_p$ is computed by picking a point in $j$ and taking the four nearest points in $p$ as a basis for a quadratic interpolation. The normalisation factor $N_{\text{over}}$ is the total number of points used to evaluate $\mathcal{E}_p$. The results are summarised in Tab. III and the corresponding curve collapse for Binder's cumulant is shown in Fig. 11.

In principle, this method could also be used for $\chi_m$, but it would be necessary to minimise for five parameters. Our investigation shows that this leads to numerical instabilities and the extraction of critical exponents from the susceptibility using this method is not possible hitherto.

|  | $T_c^{(L=\infty)}$ | $\nu$ | interval |
|---|---|---|---|
| $\kappa = 0.06$ | 18.147(24) | 0.550(1) | 17.4, 18.8 |
| $\kappa = 0.00$ | 16.667(27) | 0.525(6) | 16.0, 17.2 |
| O(4) | 0.3005(34) | 0.50000(3) | 0.294, 0.314 |

TABLE III: Curve collapse results of Binder's cumulant where the last column indicates the interval of the control parameter in which the procedure has been used. The parameter $T$ stands either for $y$ in the Higgs-Yukawa model or for $\kappa$ in the O(4) model. All errors are statistical only.
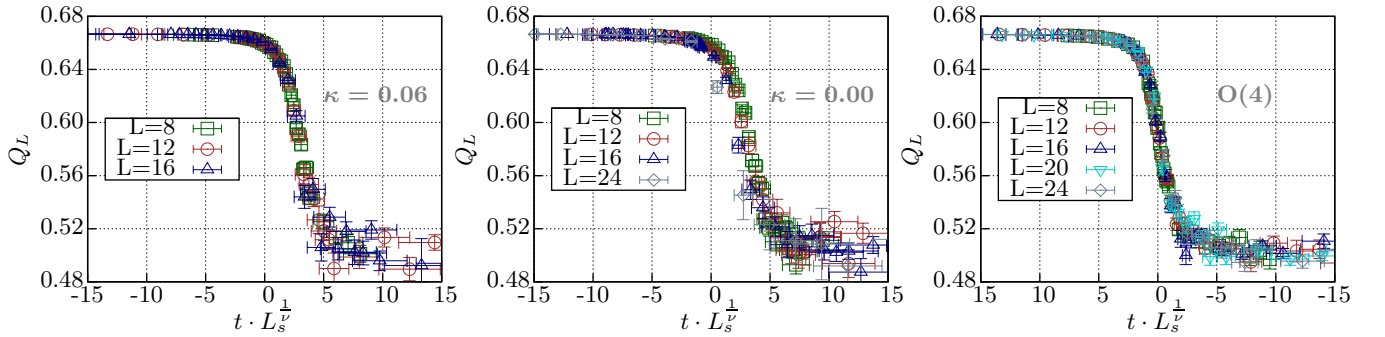


FIG. 11: Scaling behaviour of Binder's cumulant at $\kappa = 0.06$ (left), $\kappa = 0.00$ (middle) and the O(4) model (right) for various volumes using the parameters listed in table III.

At this point we can claim that we have found a second order phase transition between the SYM and the FM phases in the strong Yukawa coupling regime. The absence of discontinuities in $\langle m \rangle$ and the second-order finite size scaling of $\chi_m$ are strong evidence for such a statement. It is interesting to compare the critical exponents extracted from the susceptibility and Binder's cumulant with the ones of the weak-Yukawa model and the O(4) model.

To be able to make a direct comparison of the O(4) model with the Higgs-Yukawa model, the same strategy has been used to compute observables in the pure scalar sector of the theory. In particular, the same analysis techniques have been used. The results of the correlated fit to $\chi_m$ are summarised in Tab. II. The errors quoted there are purely statistical. Investigation of the dependence of the results on the fit interval leads to systematic uncertainties which are as large as the statistical errors roughly. It is not possible to claim a significant difference in the critical exponents between the Higgs-Yukawa model and the O(4) model from this method so far.

The curve collapse method, however, can only provide us with information about one critical exponent, namely $\nu$. The advantage of this method is the significantly smaller statistical error compared to the fit to $\chi_m$. However, it must be used with care. The scaling behaviour described in Eq. (34) is only true close to the critical point. If this method is applied at points too far away form the phase transition the result can be affected by scaling-violation effects. One possibility to achieve an impression of these effects is the dependence on the interval in which the curve collapse method is applied. It was found, that the systematic uncertainty is roughly a factor of five larger than the statistical error. However, in the case of $\kappa = 0.06$ and of the O(4) model the total error is still a factor of five smaller compared to the fitting procedure. In the case of $\kappa = 0.00$ the total errors are compatible.

The results of the critical exponent, $\nu$, in Tabs. II and III indicates that the strong-Yukawa model and the O(4) model may belong to different universality classes. However, in the procedure of using Eq. (32) to determine this exponent, the difference of the two models can be as small as two standard deviations. We stress that it is also important to investigate the scaling violation as pointed out in Refs. [62–66, 69, 70]. In particular, the observation of the multiplicative logarithmic scaling violation is directly related to the triviality of the theory [62–66, 75]. Presently, we are exploring such analyses and performing computations at additional parameter values. In the near future, we will therefore be able to see whether the value of $\nu$ in the strong bare Yukawa coupling regime is indeed different from the one of pure O(4) model. If we would find a significant difference, then it will be important to investigate the strong-coupling regime closer and, in particular, a computation of the spectrum of the Higgs-Yukawa model in the strong-coupling region will become most interesting.

### D.   Finite-temperature phase transition

One important subject in the study of the Higgs-Yukawa model is the finite-temperature phase transition. In this section we describe the status of our investigation of this transition. We are particularly interested in determining the critical temperature where the system undergoes a phase transition from the symmetric phase with vanishing scalar *vev*, $v = 0$, to the broken phase with non-vanishing $v$. Further interest lies in the determination of the order of the phase transition and the critical exponents. Results reported in this article are obtained at two values of the fermion mass, $m_f \approx 175\text{GeV}$ and $m_f \approx 700\text{GeV}$.

Choosing the boundary conditions in the Euclidean temporal direction to be periodic for bosonic and anti-periodic for fermion fields, the temperature $T$ on the lattice is given by

$$T = \frac{1}{aL_t} = \frac{\Lambda}{L_t} \tag{37}$$

where $L_t$ denotes the dimensionless temporal extent of the lattice. For the study of the finite-temperature phase transition, we work at fixed bare Yukawa couplings which lead to the desired fermion masses. Results presented here are from lattice simulations performed at $\hat{\lambda} = \infty$. To vary the temperature, we change the value of $\kappa$ at fixed $L_t$. This is equivalent to adjusting the lattice spacing while fixing the number of points in the temporal extent of the lattice corresponding then to a change in the temperature.

Our study shows that the finite-temperature phase transitions in the Higgs-Yukawa model are second-order. The order parameter is the magnetisation as defined in Eqs. (15) and (16). Since the correlation length is never divergent because of finite-volume effects, we resort to finite-size scaling techniques to investigate the second-order finite-temperature phase transition in this work. In particular, we analyse the scaling behaviour of the susceptibility of the magnetisation, Eq. (26). As in Ref. [73], we fit the susceptibility according to the partly phenomenologically motivated function

$$\chi_m(\kappa) = A \left( L_s^{-2/\nu} + B_{+/-}(\kappa - \kappa_c)^2 \right)^{-\gamma/2}, \quad \nu = 0.68, \quad \gamma = 1.38, \tag{38}$$

where $A$, $B_{+/-}$, and $\kappa_c$ are free fit parameters ($B_{+/-}$ are coefficients in the broken and the symmetric phases, respectively), and $\nu$ and $\gamma$ are the critical exponents of the three dimensional O(4) model which are expected to characterise the second-order phase transition. Note that we use the fit function of Eq. (38) with fixed values of the critical exponents only to extract the critical value of $\kappa$, denoted as $\kappa_c$ which in turn leads to the evaluation of the critical temperature. This approach is different from that used for the investigation of the strong-Yukawa model as described in Sec. IV C. Since $\kappa_c$ depends on the spatial volume, we perform simulations on various spatial lattice sizes and perform an infinite volume extrapolation using the formula ($D$ is an unknown constant),

$$\kappa_c(L) = \kappa_c(\infty) + D \cdot L^{-\nu}. \tag{39}$$

Having extracted $\kappa_c$ in the infinite-volume limit, $\kappa_c(\infty)$, we can determine the lattice spacing at this $\kappa$ value by performing zero-temperature simulations at exactly the same choice of couplings, and using Eq. (19). This then allows us to predict the critical temperature, $T_c$, through Eq. (37). In order to estimate the systematic effects in $T_c$ arising from the uncertainty in $\kappa_c$, we also carry out two additional zero-temperature simulations with $\kappa$ values chosen to reflect the error on $\kappa_c$. In this procedure, it is very challenging to maintain a constant Higgs boson mass, since it depends significantly on the $\kappa$ value. In the results presented in the following, this is indeed the case. On the other hand, we observe that the variation in $m_H$ is only $\sim 15\%$, resulting in a similar systematic uncertainty for the critical temperature.

### 1. Finite-temperature study at physical top quark mass

As the first step, we investigate the case of a degenerate fermion doublet with the quark mass close to the physical top quark mass. To this end we fix the bare Yukawa coupling according to the tree-level estimate of $y = m_t/v_r$, which has been shown to be a good approximation in this region of couplings [28]. We perform simulations at two different temporal extents ($L_t = 4, 6$) for estimating the discretisation effects. In addition, three spatial extents, $L_s = 16, 20, 24$, are implemented in order to perform the infinite-volume extrapolation.

The results of the magnetisation at $L_t = 4$ and $6$ are plotted in Fig. 12(a) and Fig. 12(d), respectively. It is obvious that there is a transition from the symmetric to the broken phase for each choice of $L_t$. The corresponding susceptibilities are shown in Figs. 12(b) and 12(e). The $L-$dependence of $\kappa_c(L)$ is well described by Eq. (39), as can be seen in Fig. 12(f). In Fig. 12(c), we depict the infinite-volume extrapolation of the cut-off scale, $\Lambda = 1/a$, for the calculations using $L_t = 4$ with three $\kappa$ values around the central value of $\kappa_c$.

Table IV summarises the current status of our finite-temperature study at a fermion mass close to physical top-quark mass. Results from two analyses using $L_t = 4$ and $6$ are shown. These two choices of the temporal extent lead to compatible results of $T_c$, indicating that the discretisation effects may be small. It should be noted that the Higgs boson mass turns out to be different in the calculations using these two choices of $L_t$. This can be resolved with more tuning and performing new simulations. In particular, we are planning zero-temperature simulations with larger spatial extent. This will allow us to have better control of the infinite-volume extrapolation. Nevertheless, our preliminary results already show that

$$m_H/T_c \sim 1, \tag{40}$$

for $m_f \sim m_t^{\text{phys}}$.

| | $\kappa_c(\infty)$ | $\Lambda(\kappa_c)$ in GeV | $T_c$ in GeV | $m_t$ in GeV | $m_H$ in GeV |
|---|---|---|---|---|---|
| $L_t = 4$ | 0.301405(38) | 2070(11) | 517.5(2.8) | 172.1(1.5) | 575(25) |
| $L_t = 6$ | 0.299561(53) | 3052(64) | 509 (11) | 173.6(2.9) | 500(25) |

TABLE IV: Results for our finite-temperature study performed at the physical top quark mass.
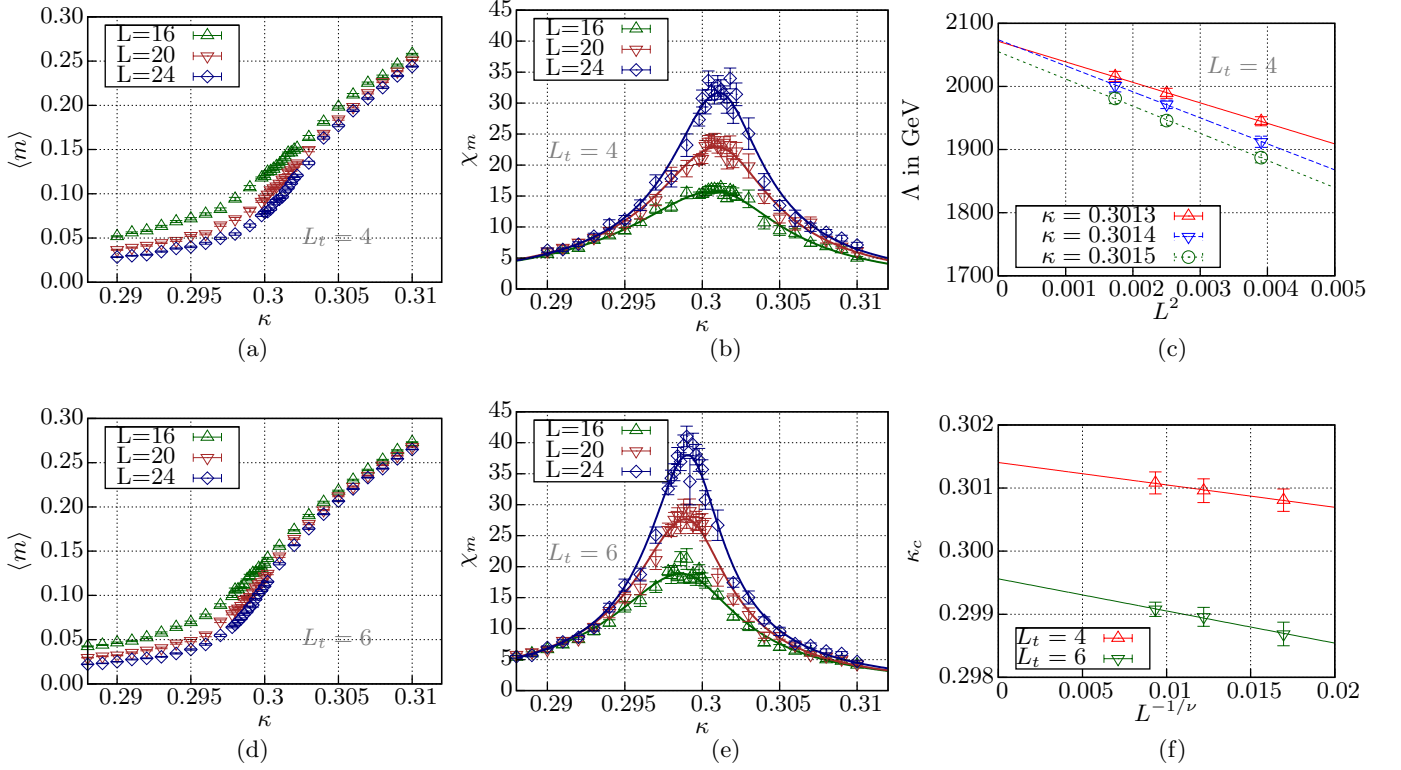
FIG. 12: Results of our finite-temperature study at the physical top quark mass with the quartic coupling $\hat{\lambda} = \infty$. Plots (a) and (d): The magnetisation for temporal extents of $L_t = 4$ and $L_t = 6$. Plots (b) and (e): The corresponding susceptibilities with the fit function in Eq. (38). Plot (c): Infinite-volume extrapolation of the cut-off scale at zero-temperature, with the $\kappa$ values close to the central value of $\kappa_c$ obtained in the $L_t = 4$ case. Plot (f): Infinite-volume extrapolation of $\kappa_c$ using Eq. (39). Note that for the case of zero temperature $L^2$ denotes $\sqrt{V_4}$ with $V_4 = L_s^3 L_t$ and $L_t = 2L_s$.

#### 2. Status of finite-temperature study at a quark mass of about 700GeV

In this section we present the status of our work on the critical temperature in the Higgs-Yukawa model with one heavy fermion doublet with a mass of about 700GeV. We follow the same strategy as in the previous section. Here the zero-temperature simulations are still in progress. Thus, the lattice spacings for this calculation are not yet available to us.

Results of the susceptibility, and the infinite-volume extrapolation for $\kappa_c$ can be found in Fig. 13. From Fig. 13(c), we notice that the values of $\kappa_c$ in the $L_t = 4$ calculation are significantly smaller than that in the $L_t = 6$ analysis. From the phase structure presented in Fig. 6 and the value of $\hat{y} \sim 2.8$, it is clear that the critical value of $\kappa$ is in the FM phase of the zero temperature theory, as expected. Comparing $\kappa_c$ for the $L_t = 4$ and $L_t = 6$ calculations, we also find that the $L_t = 4$ simulations are carried out closer to the FM−SYM phase boundary, and are thus performed at larger values of the cut-off.
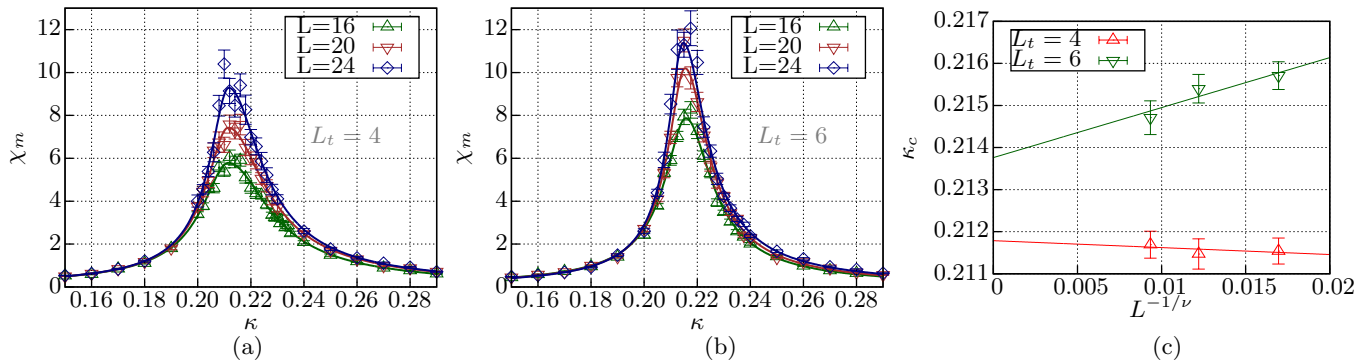
FIG. 13: Plots (a) and (b) show the susceptibility as function of $\kappa$ at the large fermion mass of about 700GeV. Plot (c) is the infinite-volume extrapolation for $\kappa_c$.

## V. OUTLOOK

In this article we have provided an overview of non-perturbative lattice calculations of the Higgs-Yukawa sector of the Standard Model and its extension with a fourth fermion generation. The phase diagram of the model has been studied and a complex and interesting structure has been revealed. At small values of the bare Yukawa coupling the properties of the phase transitions are consistent with the standard model expectation [23, 24]. However, we also establish an additional phase transition at very large values of the bare Yukawa coupling [23, 24, 31]. This offers the very interesting possibility to investigate a strongly interacting Higgs-Yukawa model. We performed a detailed study of the properties of the phase transitions at strong bare Yukawa coupling and determined the critical exponents characterising the phase transitions through a finite size scaling analysis. Although there are presently indications that these critical exponents may differ from the standard model ones, at this stage of our investigations it is too early to say that in the strong bare Yukawa coupling region indeed a non-Standard-Model-like phase structure exists.

As an interesting direction we have also examined the Higgs-Yukawa model at non-zero temperature for fermion masses ranging from 175GeV to 700GeV [57]. We find that the transition is always of second order and that the critical temperature is higher for increasing fermion mass.

For a Standard Model top quark mass we have established lower and upper Higgs boson mass bounds as a function of the (lattice) cut-off of the theory [26–28]. We also performed a detailed resonance analysis of the Higgs boson which confirmed that the Higgs boson mass bounds which assumed a stable Higgs boson are not affected by the resonance character of the Higgs boson [29]. Furthermore, we find that the Higgs boson decay width into massive Goldstone bosons is never larger than 10% of the Higgs boson mass and in good agreement with perturbative estimates. As a consequence of our lattice study of the lower and upper Higgs boson mass bounds within the Higgs-Yukawa sector at a physical value of the top quark mass, we can, in principle, estimate the energy scale at which the standard model has to break down.

We extended the study of the Higgs boson mass bound to a possible fourth generation of quarks considering fermion masses up to 700GeV [30]. We found that the upper Higgs boson mass bound shows only a moderate shift by about 20% at such a fermion mass when compared to the bound for a Standard Model top quark mass. However, the lower Higgs boson mass bound is altered significantly and can be as high as 500GeV for a fermion mass of 700GeV. We complemented our non-perturbative lattice simulations with a lattice perturbative calculation of the lower Higgs boson mass bound from the effective potential. We found a very good agreement with the lattice simulation data. This enabled us to test the stability of the lower bound against additions of higher dimensional operators. As a result we observed that the lower bound is not affected by including such additional operators. This finding puts severe constraints on the fourth generation if the particle with a mass of 125GeV seen at the LHC is the standard model Higgs boson.

Let us discuss the consequences of our lattice study of the Higgs-Yukawa sector of the standard model and its extension to a fourth fermion generation, assuming that the particle detected at the LHC [6, 7] is a Higgs boson with a mass of

125GeV. For the standard model such a Higgs boson mass leads to rather small values of the renormalised quartic and Yukawa couplings and it seems therefore that the electroweak sector of the standard model can be described perfectly within perturbation theory. Therefore, the perturbative analysis of Ref. [8] provides the result that the energy scale, up to which the Standard Model can be valid, is very high. Considering the extension of a fourth fermion generation, the lower Higgs boson mass bound together with the phenomenological lower bound of the fourth generation fermion mass provides very severe constraints on the existence of the fourth generation.

As a conclusion, our findings suggest that the electroweak theory of the Standard Model is a perfect description of particle interaction up to very high energies as discussed in Ref. [8]. Furthermore, a simple extension of the standard model by adding only a fourth fermion generation is most likely not realised. However, as discussed in Ref. [76] the addition of a singlet scalar field could change the situation. As shown in Ref. [76], the lower Higgs boson mass bound can be lowered significantly in the presence of such an additional scalar field. Of course, in Ref. [76] only a perturbative calculation has been performed for the scenario of adding such a singlet scalar field and non-perturbative calculations, such as the ones presented here, to scrutinise this picture are highly desirable.

We have demonstrated that with lattice field theory techniques generic strongly interacting Higgs-Yukawa theories can be studied in a controlled and accurate way. This became possible through a conceptual breakthrough of formulating chiral invariant theories on the lattice together with a much improved understanding of systematic effects such as finite size effects or determining resonance parameters. Since in addition the existing computing power of present super computers is clearly adequate to perform calculations of Higgs-Yukawa models, lattice computations can contribute to our understanding of Higgs-Yukawa models, in particular in the strongly interacting regime.

[1] R. F. Dashen and H. Neuberger, Phys.Rev.Lett. **50**, 1897 (1983).
[2] T. Lee and G. Wick, Phys.Rev. **D9**, 2291 (1974).
[3] A. D. Linde, JETP Lett. **23**, 64 (1976).
[4] S. Weinberg, Phys.Rev.Lett. **36**, 294 (1976).
[5] M. Sher, Phys.Rept. **179**, 273 (1989).
[6] The ATLAS Collaboration, G. Aad *et al.*, (2012), 1207.7214.
[7] The CMS Collaboration, S. Chatrchyan *et al.*, (2012), 1207.7235.
[8] G. Degrassi *et al.*, (2012), 1205.6497.
[9] M. S. Carena, A. Megevand, M. Quiros, and C. E. Wagner, Nucl.Phys. **B716**, 319 (2005), hep-ph/0410352.
[10] B. Holdom *et al.*, PMC Phys. **A3**, 4 (2009), 0904.4698.
[11] J. Smit, Nucl.Phys.Proc.Suppl. **17**, 3 (1990).
[12] J. Shigemitsu, Nucl.Phys.Proc.Suppl. **20**, 515 (1991).
[13] M. F. Golterman, Nucl.Phys.Proc.Suppl. **20**, 528 (1991).
[14] A. De and J. Jersak, Adv.Ser.Direct.High Energy Phys. **10**, 732 (1992).
[15] I. Montvay and G. Münster, *Quantum Fields on a Lattice*Cambridge Monographs on Mathematical Physics (Cambridge University Press, 1997).
[16] M. F. Golterman, D. N. Petcher, and E. Rivas, Nucl.Phys.Proc.Suppl. **29BC**, 193 (1992), hep-lat/9207005.
[17] K. Jansen, Phys.Rept. **273**, 1 (1996), hep-lat/9410018.
[18] P. H. Ginsparg and K. G. Wilson, Phys.Rev. **D25**, 2649 (1982).
[19] M. Luscher, Phys.Lett. **B428**, 342 (1998), hep-lat/9802011.
[20] T. Bhattacharya, M. R. Martin, and E. Poppitz, Phys.Rev. **D74**, 085028 (2006), hep-lat/0605003.

[21] J. Giedt and E. Poppitz, JHEP **0710**, 076 (2007), hep-lat/0701004.
[22] E. Poppitz and Y. Shang, JHEP **0708**, 081 (2007), 0706.1043.
[23] P. Gerhold and K. Jansen, JHEP **0709**, 041 (2007), 0705.2539.
[24] P. Gerhold and K. Jansen, JHEP **0710**, 001 (2007), 0707.3849.
[25] Z. Fodor, K. Holland, J. Kuti, D. Nogradi, and C. Schroeder, PoS **LAT2007**, 056 (2007), 0710.3151.
[26] P. Gerhold and K. Jansen, JHEP **0907**, 025 (2009), 0902.4135.
[27] P. Gerhold, PhD thesis, arXiv:1002.2569.
[28] P. Gerhold and K. Jansen, JHEP **1004**, 094 (2010), 1002.4336.
[29] P. Gerhold, K. Jansen, and J. Kallarackal, Phys.Lett. **B710**, 697 (2012), 1111.4789.
[30] P. Gerhold, K. Jansen, and J. Kallarackal, JHEP **1101**, 143 (2011), 1011.1648.
[31] J. Bulava *et al.*, PoS **LATTICE2011**, 075 (2011), 1111.4544.
[32] ALPHA collaboration, U. Wolff, Comput.Phys.Commun. **156**, 143 (2004), hep-lat/0306017.
[33] H. Neuberger, Phys.Lett. **B417**, 141 (1998), hep-lat/9707022.
[34] H. Neuberger, Phys.Lett. **B427**, 353 (1998), hep-lat/9801031.
[35] P. Hernandez, K. Jansen, and M. Luscher, Nucl.Phys. **B552**, 363 (1999), hep-lat/9808010.
[36] R. Frezzotti and K. Jansen, Phys.Lett. **B402**, 328 (1997), hep-lat/9702016.
[37] R. Frezzotti and K. Jansen, Nucl.Phys. **B555**, 395 (1999), hep-lat/9808011.
[38] R. Frezzotti and K. Jansen, Nucl.Phys. **B555**, 432 (1999), hep-lat/9808038.
[39] P. Gerhold and K. Jansen, PoS **LAT2009**, 054 (2009), 0912.0407.
[40] S. Hashimoto, PoS **LATTICE2008**, 011 (2008), 0811.1257.
[41] A. Hasenfratz *et al.*, Z.Phys. **C46**, 257 (1990).
[42] A. Hasenfratz *et al.*, Nucl.Phys. **B356**, 332 (1991).
[43] M. Gockeler and H. Leutwyler, Nucl.Phys. **B361**, 392 (1991).
[44] J. Kallarackal, PhD thesis.
[45] U. M. Heller, M. Klomfass, H. Neuberger, and P. M. Vranas, Nucl.Phys. **B405**, 555 (1993), hep-ph/9303215.
[46] A. Denner *et al.*, Eur.Phys.J. **C72**, 1992 (2012), 1111.6395.
[47] M. S. Chanowitz, M. Furman, and I. Hinchliffe, Nucl.Phys. **B153**, 402 (1979).
[48] M. S. Chanowitz, M. Furman, and I. Hinchliffe, Phys.Lett. **B78**, 285 (1978).
[49] M. Luscher and P. Weisz, Nucl.Phys. **B318**, 705 (1989).
[50] A. Hasenfratz, K. Jansen, C. B. Lang, T. Neuhaus, and H. Yoneyama, Phys.Lett. **B199**, 531 (1987).
[51] J. Kuti, L. Lin, and Y. Shen, Phys.Rev.Lett. **61**, 678 (1988).
[52] A. Hasenfratz *et al.*, Nucl.Phys. **B317**, 81 (1989).
[53] M. Luscher, Nucl.Phys. **B354**, 531 (1991).
[54] M. Luscher, Nucl.Phys. **B364**, 237 (1991).
[55] K. Rummukainen and S. A. Gottlieb, Nucl.Phys. **B450**, 397 (1995), hep-lat/9503028.
[56] X. Feng, K. Jansen, and D. B. Renner, Phys.Rev. **D83**, 094505 (2011), 1011.5288.
[57] J. Bulava, P. Gerhold, K. Jansen, J. Kallarackal, and A. Nagy, PoS **LATTICE2011**, 301 (2011), 1111.2792.
[58] A. Abada and R. Shrock, Phys.Rev. **D43**, 304 (1991).
[59] A. Hasenfratz, P. Hasenfratz, K. Jansen, J. Kuti, and Y. Shen, Nucl.Phys. **B365**, 79 (1991).
[60] A. G. Cohen, D. Kaplan, and A. Nelson, Ann.Rev.Nucl.Part.Sci. **43**, 27 (1993), hep-ph/9302210.
[61] M. E. Fisher and M. N. Barber, Phys.Rev.Lett. **28**, 1516 (1972).
[62] E. Brezin, J.Phys.(France) **43**, 15 (1982).
[63] E. Brezin and J. Zinn-Justin, Nucl.Phys. **B257**, 867 (1985).
[64] W. Bernreuther and M. Gockeler, Nucl.Phys. **B295**, 199 (1988).
[65] R. Kenna and C. Lang, Nucl.Phys. **B393**, 461 (1993), hep-lat/9210009.
[66] R. Kenna, Nucl.Phys. **B691**, 292 (2004), hep-lat/0405023.
[67] K. Binder, Z.Phys. **B43**, 119 (1981).
[68] B. A. Freedman and J. Baker, George A., (1982).
[69] V. Privman and M. Fisher, J.Phys.A **A16**, L295 (1983).
[70] K. Binder, M. Nauenberg, V. Privman, A. P. Young, Phys.Rev. **B31** (1985) 1498.
[71] E. Focht, J. Jersak, and J. Paul, Phys.Rev. **D53**, 4616 (1996), hep-lat/9511005.
[72] O. Eberhardt *et al.*, (2012), 1209.1101.
[73] K. Jansen and P. Seuferling, Nucl.Phys. **B343**, 507 (1990).
[74] S. M. Bhattacharjee and F. Seno, J.Phys.A:Math.Gen. **34**, 6375 (2001).
[75] M. Aizenman and R. Graham, Nucl.Phys. **B225**, 261 (1983).
[76] J. Elias-Miro, J. R. Espinosa, G. F. Giudice, H. M. Lee, and A. Strumia, JHEP **1206**, 031 (2012), 1203.0237.